East Asian Journal on Applied Mathematics
doi: 10.4208/eajam.2024-195.010325

Vol. **16**, No. 1, pp. 105-128
February 2026

High-Order Operator-Compensation Schemes with Mass and Energy Conservation for the Multi-Dimensional Zakharov System

Yanjing Li[1], Xianggui Li[1], Dongying Hua[1] and Yongyong Cai[2,*]

[1]*School of Applied Science, Beijing Information Science and Technology University, Beijing 100192, China.*
[2]*Laboratory of Mathematics and Complex Systems (Ministry of Education), School of Mathematical Sciences, Beijing Normal University, Beijing 100875, China.*

Received 21 November 2024; Accepted (in revised version) 1 March 2025.

Abstract. This paper presents high-order operator-compensation (OC) methods and the Crank-Nicolson (CN) technology to solve the Zakharov system (ZS). Firstly, the OC method is used for spatial discretization, and semi-discrete high-order OC schemes are obtained, which can maintain mass and energy conservation. Subsequently, the CN technology is adopted for temporal discretization, and full-discrete high-order OC schemes are obtained, which can inherit mass and energy conservation and achieve arbitrary even-order accuracy in space and second-order accuracy in time. In the process of solving ZS, we employ the linearization method to handle the nonlinear ZS, which significantly improves the computational efficiency. Considering the large stencil of numerical schemes, we propose a fast numerical iterative method to deal with the problem, which saves the computational cost. Numerical experiments are given to test accuracy order, verify conservation property, and simulate dynamic evolution.

AMS subject classifications: 65M06, 65M20, 35L70, 35Q55

Key words: Zakharov system, high-order operator-compensation method, conservation, Crank-Nicolson technology.

1. Introduction

Zakharov system is a nonlinear coupled wave equation describing the interaction of high-frequency Langmuir waves and low-frequency ionic acoustic waves in plasma. It is regarded as a general model for controlling the interaction between dispersive and non-dispersive waves [27]. The standard dimensionless form of ZS is

$$i\Psi_t + \Delta\Psi = W\Psi, \qquad \mathbf{x}\in\mathbb{R}^d, \quad t>0, \tag{1.1}$$

$$W_{tt} - \Delta W = \Delta(|\Psi|^2), \quad \mathbf{x}\in\mathbb{R}^d, \quad t>0, \tag{1.2}$$

*Corresponding author. *Email address:* yongyong.cai@bnu.edu.cn (Y. Cai)

where $i = \sqrt{-1}$ is the imaginary unit, $d = 1, 2, 3$ the spatial dimension, $\mathbf{x}$ the spatial coordinate, t the time variable, Δ the d-dimensional Laplace operator, $\Psi := \Psi(\mathbf{x}, t)$ unknown complex function representing the envelope of a high-frequency electric field, and $W := W(\mathbf{x}, t)$ unknown real function representing the deviation of the ion density from its equilibrium value. The initial conditions are

$$\Psi(\mathbf{x}, 0) = \Psi_0(\mathbf{x}), \quad W(\mathbf{x}, 0) = W_0(\mathbf{x}), \quad W_t(\mathbf{x}, 0) = \omega(\mathbf{x}), \quad \mathbf{x} \in \mathbb{R}^d, \tag{1.3}$$

where $\Psi_0(\mathbf{x})$ represents a given smooth complex function, $W_0(\mathbf{x})$ and $\omega(\mathbf{x})$ represent two given smooth real functions.

The Zakharov system possesses the two essential conservation quantities — i.e. the mass

$$M(t) := \int_{\mathbb{R}^d} |\Psi(\mathbf{x}, t)|^2 d\mathbf{x} \equiv M(0), \quad \mathbf{x} \in \mathbb{R}^d, \quad t > 0$$

and the energy

$$\begin{aligned} E(t) := & \int_{\mathbb{R}^d} |\nabla \Psi(\mathbf{x}, t)|^2 d\mathbf{x} + \frac{1}{2} \int_{\mathbb{R}^d} |\nabla u(\mathbf{x}, t)|^2 d\mathbf{x} \\ & + \frac{1}{2} \int_{\mathbb{R}^d} |W(\mathbf{x}, t)|^2 d\mathbf{x} + \int_{\mathbb{R}^d} |\Psi(\mathbf{x}, t)|^2 W(\mathbf{x}, t) d\mathbf{x} \\ \equiv & E(0), \quad t > 0, \end{aligned}$$

where the intermediate variable $u(\mathbf{x}, t)$ satisfies

$$\Delta u = W_t, \quad \mathbf{x} \in \mathbb{R}^d, \quad t > 0.$$

This system is applied in various fields such as plasma physics, fluid mechanics, and new energy. However, since the ZS is nonlinear, obtaining its analytical solutions for general initial conditions is challenging. It is necessary to study and solve the system through numerical methods.

Mathematically speaking, ZS can be seen as the coupling of the Schrödinger equation (1.1) and the wave equation (1.2). In theoretical analysis, there are numerous studies of the ZS — cf. [1, 16, 19, 20]. The global existence of weak solutions and the existence and uniqueness of smooth solutions with given smooth initial values for one-dimensional ZS were proven in [24]. Later, researchers improved the well posedness of ZS [5] and extended it to the case of generalized nonlinearity [10].

Extensive numerical research has been conducted on the ZS. Payne *et al.* [22] proposed the Fourier spectral method for the one-dimensional ZS, which suppresses aliasing errors by using only two-thirds of the Fourier components for a specific grid during fast Fourier transform. Glassey [11, 12] proposed an implicit finite difference scheme that could preserve energy conservation and proved its convergence in order $\mathcal{O}(h + \tau)$. A conservative difference scheme for ZS, which was implicit or semi-explicit depending on parameter choice,

was proposed by Chang and Jiang [9]. Optimal second-order convergence in time and space was established by them and it was extended to the generalized ZS [8]. The time-splitting spectral method and the local spectral method were proposed by Bao *et al.* [4]. Various numerical methods, such as the Fourier pseudo-spectral method, were compared by them to analyze the generalized ZS and improve the accuracy. Cai *et al.* [6] proposed a fourth-order compact finite difference method to study the quantum ZS that could maintain mass and energy conservation. Later, multi-symplectic numerical methods [25], locally discontinuous Galerkin methods [26], exponential-wave-integral spectral methods [4], and time-splitting spectral methods [4,15] were introduced to solve ZS. In recent years, several numerical methods have been developed and analyzed ZS in the subsonic limit [2,3,7,23]. There have been more numerical studies on ZS and soliton collisions in [13,14,21].

High-order conservative OC schemes have drawn more attention since they can provide fine physical details for ZS. This paper proposes high-order conservative OC schemes for the multi-dimensional ZS based on the OC method which was first presented to solve the Gross-Pitaevskii equation [18]. High-order numerical schemes can maintain mass and energy conservation while achieving arbitrary even-order accuracy in space and second-order accuracy in time. In the process of calculation, a linearization solution technology is designed for the full-discrete high-order OC schemes for the nonlinear ZS. This simplifies the complexity of the problem, making it easier to solve and greatly improving computational efficiency. At the same time, in the process of solving full-discrete high-order OC schemes, a numerical iteration method is proposed to deal with the complicated system of linear algebraic equations which results from the large stencil. This method can save the computational cost.

This paper is organized as follows. In Section 2, we introduce high-order compensation operators for spatial discretization. We obtain semi-discrete high-order OC schemes and prove the conservation of mass and energy. Furthermore, the CN technology is adopted for temporal discretization. Full-discrete high-order OC schemes are obtained that can maintain mass and energy conservation. The linearized solution technology and the numerical iterative method are also given. In Section 3, we provide the numerical results to test the accuracy order, verify the conservation property, and simulate dynamic behaviors. In Section 4, some conclusions are drawn.

2. Numerical Method for Zakharov System

Here we focus on high-order OC methods for two-dimensional ZS, which can be directly generalized to the three-dimensional case. In practical applications, variable (x,y) is typically defined over the entire space $\mathbb{R}^2$. However, for computational purposes, we confine to a sufficiently large bounded domain $\Omega=[x_L,x_R]\times[y_L,y_R]$, and subject to the boundary condition $\Psi(x,t)=0, W(x,t)=0$ on $\partial\Omega, t>0$. The ZS (1.1)-(1.3) is transformed into the initial-boundary value problem. Now let us consider the general two-dimensional ZS with periodic initial-boundary conditions

$$i\Psi_t+\Psi_{xx}+\Psi_{yy}=W\Psi,\quad t\in(0,T],\quad (x,y)\in\Omega, \tag{2.1}$$

$$W_{tt}-(W_{xx}+W_{yy})=\frac{\partial^2(|\Psi|^2)}{\partial x^2}+\frac{\partial^2(|\Psi|^2)}{\partial y^2}, \qquad t\in(0,T], \quad (x,y)\in\Omega, \tag{2.2}$$

$$\Psi(x,y,0)=\Psi_0(x,y), \ \ W(x,y,0)=W_0(x,y), \ \ W_t(x,y,0)=\omega(x,y), \quad (x,y)\in\Omega, \tag{2.3}$$

where $\Psi_0(x,y), W_0(x,y)$ and $\omega(x,y)$ are smooth integrable functions, and periodic boundary conditions for W and Ψ are imposed. For the consistency of initial data, we assume $\omega(x,y)$ satisfies $\iint_\Omega \omega(x,y)dxdy=0$. Eqs. (2.1)-(2.3) have two important conserved quantities — i.e. the mass

$$M(t):=\iint_\Omega |\Psi(x,y,t)|^2dxdy\equiv M(0), \quad t\in(0,T],$$

and the energy

$$\begin{aligned}E(t):=&\iint_\Omega |\nabla\Psi(x,y,t)|^2dxdy+\frac{1}{2}\iint_\Omega |\nabla u(x,y,t)|^2dxdy\\&+\frac{1}{2}\iint_\Omega |W(x,y,t)|^2dxdy+\iint_\Omega |\Psi(x,y,t)|^2W(x,y,t)dxdy\\\equiv& E(0), \quad t\in(0,T],\end{aligned}$$

where the intermediate variable $u(x,y,t)$ satisfies $\iint_\Omega u(x,y,t)dxdy=0$ and

$$u_{xx}+u_{yy}=W_t, \quad (x,y)\in\Omega, \quad t\in(0,T].$$

Noticing that $\iint_\Omega \omega(x,y)dxdy$ leads to $\iint_\Omega W_t dxdy=0$, it becomes evident that the intermediate variable $u(x,y,t)$ is uniquely defined.

Before constructing high-order OC schemes of ZS, some notations are introduced. We divide the domain Ω in the x-direction equally by selecting a positive integer J. The spatial mesh size in the x-direction is $h_x=(x_R-x_L)/J$. Similarly, for a given positive integer K, the spatial mesh size in the y-direction is $h_y=(y_R-y_L)/K$. For a given positive integer N, the time step size is $\tau=T/N$. The set of the spatial grid points is

$$\Omega_h=\big\{(x_j,y_k)\mid x_j=x_L+jh_x,\ j=0,1,2,\ldots,J-1, y_k=y_L+kh_y,\ k=0,1,2,\ldots,K-1\big\}.$$

The time steps can be expressed as $t_n=n\tau, (0\le n\le N)$. We denote the index set

$$\Theta_{JK}=\big\{(j,k)\mid j=0,1,2,\ldots,J-1,\ k=0,1,2,\ldots,K-1\big\}$$

and introduce the complex periodic grid function space

$$P_h=\big\{\psi_h\mid \psi_h=\psi_{j,k}\in\mathbb{C}^{JK},(j,k)\in\Theta_{JK}\big\}$$

and real periodic grid function space

$$Q_h=\big\{\varphi_h\mid \varphi_h=\varphi_{j,k}\in\mathbb{R}^{JK},(j,k)\in\Theta_{JK}\big\}\subset P_h.$$

When the index range exceeds Θ_{JK}, the element ψ_h in P_h satisfies $\psi_{j\pm J,k\pm K}=\psi_{j,k}$. $\Psi^n_{j,k}$ and $W^n_{j,k}$ represent the numerical approximation of $\Psi(x_j,y_k,t_n)$ and $W(x_j,y_k,t_n)$ respectively. Denote

$$\Psi^n_h=\left\{\Psi^n_{j,k},(j,k)\in\Theta_{JK}\right\}\subset P_h,\quad W^n_h=\left\{W^n_{j,k},(j,k)\in\Theta_{JK}\right\}\subset Q_h$$

as numerical solution vectors at time $t=t_n$.

For grid functions, we introduce the following difference operators:

$$\begin{aligned}
&\delta_t^+\psi^n_{j,k}=\frac{\psi^{n+1}_{j,k}-\psi^n_{j,k}}{\tau},\qquad \delta_t^-\psi^n_{j,k}=\frac{\psi^n_{j,k}-\psi^{n-1}_{j,k}}{\tau},\\
&\delta_t^2\psi^n_{j,k}=\delta_t^+\delta_t^-\psi^n_{j,k}=\frac{\psi^{n+1}_{j,k}-2\psi^n_{j,k}+\psi^{n-1}_{j,k}}{\tau^2},\quad \psi^{n+1/2}_{j,k}=\frac{\psi^{n+1}_{j,k}+\psi^n_{j,k}}{2},\\
&\delta_x^+\psi^n_{j,k}=\frac{\psi^n_{j+1,k}-\psi^n_{j,k}}{h_x},\quad \delta_x^2\psi^n_{j,k}=\frac{\psi^n_{j+1,k}-2\psi^n_{j,k}+\psi^n_{j-1,k}}{h_x^2},\\
&\delta_y^+\psi^n_{j,k}=\frac{\psi^n_{j,k+1}-\psi^n_{j,k}}{h_y},\quad \delta_y^2\psi^n_{j,k}=\frac{\psi^n_{j,k+1}-2\psi^n_{j,k}+\psi^n_{j,k-1}}{h_y^2}.
\end{aligned}$$

By the Taylor expansion, we have

$$\partial_{xx}\psi\big|_{(x_j,y_k,t)}=C^x_\mu\psi(x_j,y_k,t)+\mathscr{O}\left(h_x^{2(\mu+1)}\right),\quad C^x_\mu=B^x_\mu\delta_x^2,$$

where the difference operators B^x_μ are defined by

$$B^x_\mu=1+a_1h_x^2\delta_x^2+a_2h_x^4\delta_x^4+\cdots+a_\mu h_x^{2\mu}\delta_x^{2\mu}$$

with the coefficients a_l, $l=1,2,\ldots$ having the form

$$a_l=\frac{(-1)^l}{2^{2l}}\sum_{j=1}^{l}\frac{(2j-1)!!\cdot(2(l-j)-1)!!}{(2j)!!\cdot(2(l-j))!!}\frac{1}{(2j+1)(2l-2j+1)}.\tag{2.4}$$

Similarly, the definition of C^y_μ is as follows:

$$C^y_\mu=B^y_\mu\delta_y^2,\quad B^y_\mu=1+a_1h_y^2\delta_y^2+a_2h_y^4\delta_y^4+\cdots+a_\mu h_y^{2\mu}\delta_y^{2\mu}.$$

It can be easily proven that B^x_μ and B^y_μ are symmetric and positive definite, while $-C^x_\mu$ and $-C^y_\mu$ are symmetric and semi-positively definite [18].

2.1. Semi-discrete schemes

By applying high-order OC methods to the spatial discretization of Zakharov system (2.1)-(2.3), semi-discrete high-order OC schemes can be written as

$$i\frac{d\Psi_{j,k}(t)}{dt}+C^x_\mu\Psi_{j,k}+C^y_\mu\Psi_{j,k}=W_{j,k}\Psi_{j,k},\qquad (j,k)\in\Theta_{JK},\quad t\in(0,T],\tag{2.5}$$

$$\frac{d^2W_{j,k}(t)}{dt^2}-C^x_\mu W_{j,k}-C^y_\mu W_{j,k}=C^x_\mu|\Psi_{j,k}|^2+C^y_\mu|\Psi_{j,k}|^2,\quad (j,k)\in\Theta_{JK},\quad t\in(0,T]\tag{2.6}$$

with the initial conditions

$$\Psi_{j,k}(0)=\Psi_0(x_j,y_k),\quad W_{j,k}(0)=W_0(x_j,y_k),\quad W_t(0)=\omega(x_j,y_k),\quad (j,k)\in\Theta_{JK}. \tag{2.7}$$

For consistency, we make the assumption that

$$\sum_{j=0}^{J-1}\sum_{k=0}^{K-1}\omega(x_j,y_k)=0,$$

which yields

$$\sum_{j=0}^{J-1}\sum_{k=0}^{K-1}W_t(x_j,y_k,t)=0,\quad t\geq 0.$$

Then we shall analyze two important properties of semi-discrete high-order OC schemes. Discrete inner product and discrete norm are defined as follows. For any grid function $\psi_h,\phi_h\in P_h$, we have

$$\langle\psi_h,\phi_h\rangle_H=h_xh_y\sum_{j=0}^{J-1}\sum_{k=0}^{K-1}\psi_{j,k}\overline{\phi_{j,k}},\quad \|\psi_h\|_H^2=\langle\psi_h,\psi_h\rangle_H,\quad \|\psi_h\|_\infty=\max_{(j,k)\in\Theta_{JK}}|\psi_{j,k}|,$$

where $\overline{\psi_{j,k}}$ is the complex conjugate of $\psi_{j,k}$. In addition, the definitions of B norm and semi-B norm are also given

$$\begin{aligned}
\|\psi_h\|_B^2&=\left\langle B_\mu^x\psi_h,\psi_h\right\rangle_H+\left\langle B_\mu^y\psi_h,\psi_h\right\rangle_H,\\
\left\|\delta_x^+\psi_h\right\|_B^2&=\left\langle -B_\mu^x\delta_x^2\psi_h,\psi_h\right\rangle_H,\\
\left\|\delta_y^+\psi_h\right\|_B^2&=\left\langle -B_\mu^y\delta_y^2\psi_h,\psi_h\right\rangle_H.
\end{aligned}$$

Theorem 2.1. *Semi-discrete high-order OC schemes* (2.5)-(2.7) *can keep mass conservation*

$$\frac{d}{dt}M_h(t)=0,\quad M_h(t)=\|\Psi_h(t)\|_H^2.$$

Proof. Calculating the discrete inner product of (2.5) with Ψ_h and taking the imaginary part, we obtain

$$\mathrm{Im}\left\langle i\frac{d\Psi_h(t)}{dt},\Psi_h\right\rangle_H+\mathrm{Im}\left\langle C_\mu^x\Psi_h,\Psi_h\right\rangle_H+\mathrm{Im}\left\langle C_\mu^y\Psi_h,\Psi_h\right\rangle_H=\mathrm{Im}\,\langle W_h\Psi_h,\Psi_h\rangle_H. \tag{2.8}$$

Due to the symmetry of C_μ^x and C_μ^y, through simple calculations, we obtain

$$\mathrm{Im}\left\langle i\frac{d\Psi_h(t)}{dt},\Psi_h\right\rangle_H=\mathrm{Re}\left\langle\frac{d\Psi_h(t)}{dt},\Psi_h\right\rangle_H=\frac{1}{2}\frac{d\,\|\Psi_h(t)\|_H^2}{dt}, \tag{2.9}$$

$$\mathrm{Im}\left\langle C_\mu^x\Psi_h,\Psi_h\right\rangle_H=0,\quad \mathrm{Im}\left\langle C_\mu^y\Psi_h,\Psi_h\right\rangle_H=0,\quad \mathrm{Im}\,\langle W_h\Psi_h,\Psi_h\rangle_H=0. \tag{2.10}$$

Substituting (2.9)-(2.10) into (2.8) yields

$$\frac{d\|\Psi_h(t)\|_H^2}{dt}=0.$$

The proof is complete. □

Theorem 2.2. *Semi-discrete high-order OC schemes* (2.5)-(2.7) *can maintain energy conservation*

$$E_h(t):=\left\|\delta_x^+\Psi_h(t)\right\|_B^2+\left\|\delta_y^+\Psi_h(t)\right\|_B^2+\frac{1}{2}\left\|\delta_x^+u_h(t)\right\|_B^2+\frac{1}{2}\left\|\delta_y^+u_h(t)\right\|_B^2$$
$$+\frac{1}{2}\|W_h(t)\|_H^2+h_xh_y\sum_{j=0}^{J-1}\sum_{k=0}^{K-1}W_{j,k}(t)\left|\Psi_{j,k}(t)\right|^2\equiv E_h(0),$$

where the intermediate variable u_h *satisfies* $\langle u_h,1\rangle_H=0$,

$$C_\mu^xu_{j,k}+C_\mu^yu_{j,k}=\frac{dW_{j,k}}{dt},\quad (j,k)\in\Theta_{JK}. \tag{2.11}$$

Proof. Calculating the discrete inner product of (2.5) with $d\Psi_h(t)/dt$ and then taking the real part, we can obtain

$$\begin{aligned}&\mathrm{Re}\left\langle i\frac{d\Psi_h(t)}{dt},\frac{d\Psi_h(t)}{dt}\right\rangle_H+\mathrm{Re}\left\langle C_\mu^x\Psi_h,\frac{d\Psi_h(t)}{dt}\right\rangle_H+\mathrm{Re}\left\langle C_\mu^y\Psi_h,\frac{d\Psi_h(t)}{dt}\right\rangle_H\\&=\mathrm{Re}\left\langle W_h\Psi_h,\frac{d\Psi_h(t)}{dt}\right\rangle_H.\end{aligned} \tag{2.12}$$

Due to the symmetry properties of C_μ^x and C_μ^y, it is easy to see

$$2\,\mathrm{Re}\left\langle i\frac{d\Psi_h(t)}{dt},\frac{d\Psi_h(t)}{dt}\right\rangle_H=0,\quad 2\,\mathrm{Re}\left\langle C_\mu^x\Psi_h,\frac{d\Psi_h(t)}{dt}\right\rangle_H=-\frac{d}{dt}\left\|\delta_x^+\Psi_h(t)\right\|_B^2, \tag{2.13}$$

$$2\,\mathrm{Re}\left\langle C_\mu^y\Psi_h,\frac{d\Psi_h(t)}{dt}\right\rangle_H=-\frac{d}{dt}\left\|\delta_y^+\Psi_h(t)\right\|_B^2, \tag{2.14}$$

$$2\,\mathrm{Re}\left\langle W_h\Psi_h,\frac{d\Psi_h(t)}{dt}\right\rangle_H=\left\langle W_{j,k}(t)\frac{d\left|\Psi_{j,k}(t)\right|^2}{dt},1\right\rangle_H. \tag{2.15}$$

Substituting (2.13)-(2.15) into (2.12), we can get

$$\frac{d}{dt}\left\|\delta_x^+\Psi_h(t)\right\|_B^2+\frac{d}{dt}\left\|\delta_y^+\Psi_h(t)\right\|_B^2+h_xh_y\sum_{j=0}^{J-1}\sum_{k=0}^{K-1}W_{j,k}(t)\frac{d|\Psi_{j,k}(t)|^2}{dt}=0. \tag{2.16}$$

Calculating the discrete inner product of (2.6) with u_h gives

$$\begin{aligned}&\left\langle\frac{d^2W_h(t)}{dt^2},u_h\right\rangle_H-\left\langle C_\mu^xW_h,u_h\right\rangle_H-\left\langle C_\mu^yW_h,u_h\right\rangle_H\\&=\left\langle C_\mu^x|\Psi_h|^2,u_h\right\rangle_H+\left\langle C_\mu^y|\Psi_h|^2,u_h\right\rangle_H.\end{aligned} \tag{2.17}$$

According to (2.11), we obtain

$$\begin{aligned}
&\left\langle \frac{d^2W_h(t)}{dt^2}, u_h \right\rangle_H \\
&= \left\langle \frac{dC_\mu^x u_h(t)}{dt} + \frac{dC_\mu^y u_h(t)}{dt}, u_h \right\rangle_H \\
&= -\frac{1}{2}\frac{d}{dt}\left\|\delta_x^+ u_h(t)\right\|_B^2 - \frac{1}{2}\frac{d}{dt}\left\|\delta_y^+ u_h(t)\right\|_B^2, \qquad (2.18)
\end{aligned}$$

$$\begin{aligned}
&\left\langle C_\mu^x W_h, u_h \right\rangle_H + \left\langle C_\mu^y W_h, u_h \right\rangle_H \\
&= \left\langle W_h, C_\mu^x u_h \right\rangle_H + \left\langle W_h, C_\mu^y u_h \right\rangle_H = \frac{1}{2}\frac{d}{dt}\|W_h(t)\|_H^2, \qquad (2.19)
\end{aligned}$$

$$\begin{aligned}
&\left\langle C_\mu^x |\Psi_h|^2, u_h \right\rangle_H + \left\langle C_\mu^y |\Psi_h|^2, u_h \right\rangle_H \\
&= \left\langle |\Psi_h|^2, C_\mu^x u_h \right\rangle_H + \left\langle |\Psi_h|^2, C_\mu^y u_h \right\rangle_H \\
&= \left\langle |\Psi_h|^2, C_\mu^x u_h + C_\mu^y u_h \right\rangle_H = \left\langle |\Psi_h|^2, \frac{dW_h}{dt} \right\rangle_H \\
&= h_x h_y \sum_{j=0}^{J-1}\sum_{k=0}^{K-1} \left|\Psi_{j,k}(t)\right|^2 \frac{dW_{j,k}(t)}{dt}. \qquad (2.20)
\end{aligned}$$

Substituting (2.18)-(2.20) into (2.17), we get

$$\begin{aligned}
&\frac{1}{2}\frac{d}{dt}\left\|\delta_x^+ u_h(t)\right\|_B^2 + \frac{1}{2}\frac{d}{dt}\left\|\delta_y^+ u_h(t)\right\|_B^2 + \frac{1}{2}\frac{d}{dt}\|W_h(t)\|_H^2 \\
&\quad + h_x h_y \sum_{j=0}^{J-1}\sum_{k=0}^{K-1} |\Psi_{j,k}(t)|^2 \frac{dW_{j,k}(t)}{dt} = 0. \qquad (2.21)
\end{aligned}$$

Summing (2.16) and (2.21), we have

$$\begin{aligned}
&\frac{d}{dt}\left\|\delta_x^+ \Psi_h(t)\right\|_B^2 + \frac{d}{dt}\left\|\delta_y^+ \Psi_h(t)\right\|_B^2 + \frac{1}{2}\frac{d}{dt}\left\|\delta_x^+ u_h(t)\right\|_B^2 \\
&\quad + \frac{1}{2}\frac{d}{dt}\left\|\delta_y^+ u_h(t)\right\|_B^2 + \frac{1}{2}\frac{d}{dt}\|W_h(t)\|_H^2 \\
&\quad + h_x h_y \sum_{j=0}^{J-1}\sum_{k=0}^{K-1} W_{j,k}(t)\frac{d\left|\Psi_{j,k}(t)\right|^2}{dt} + h_x h_y \sum_{j=0}^{J-1}\sum_{k=0}^{K-1} \left|\Psi_{j,k}(t)\right|^2 \frac{dW_{j,k}(t)}{dt} = 0,
\end{aligned}$$

i.e. $(d/dt)E_h(t) = 0$. The proof is complete. □

2.2. Fully-discrete schemes

By using the CN technology to discretize the time of semi-discrete high-order OC schemes (2.5)-(2.7), fully-discrete high-order OC schemes for $(j,k) \in \Theta_{JK}$ and $n = 0, 1, \ldots, N-1$

can be written as

$$\begin{aligned} &i\delta_t{}^{+}\Psi_{j,k}^{n}+\frac{1}{2}C_\mu^x\big(\Psi_{j,k}^{n+1}+\Psi_{j,k}^{n}\big)+\frac{1}{2}C_\mu^y\big(\Psi_{j,k}^{n+1}+\Psi_{j,k}^{n}\big)\\ &=\frac{1}{4}\big(W_{j,k}^{n+1}+W_{j,k}^{n}\big)\big(\Psi_{j,k}^{n+1}+\Psi_{j,k}^{n}\big), \end{aligned} \tag{2.22}$$

$$\begin{aligned} &\delta_t^2 W_{j,k}^{n}-\frac{1}{2}\Big(C_\mu^x\big(W_{j,k}^{n+1}+W_{j,k}^{n-1}\big)+C_\mu^y\big(W_{j,k}^{n+1}+W_{j,k}^{n-1}\big)\Big)\\ &=C_\mu^x\big|\Psi_{j,k}^{n}\big|^2+C_\mu^y\big|\Psi_{j,k}^{n}\big|^2 \end{aligned} \tag{2.23}$$

with initial conditions

$$\Psi_{j,k}^{0}=\Psi_0(x_j,y_k),\quad W_{j,k}^{0}=W_0(x_j,y_k),\quad \frac{1}{2\tau}\big(W_{j,k}^{1}-W_{j,k}^{-1}\big)=\omega(x_j,y_k). \tag{2.24}$$

The initialization satisfies $\sum_{j=0}^{J-1}\sum_{k=0}^{K-1}\omega(x_j,y_k)=0$ (consistency of initial data).

Numerical schemes (2.22)-(2.24) are abbreviated as CNOC schemes. These schemes are called CNOC2, CNOC4, CNOC6, ... when $\mu=0,1,2,\ldots$. The spatial accuracy of these schemes can achieve second-order, fourth-order, sixth-order, ..., and the temporal accuracy can achieve second-order. Theoretically, CNOC schemes can achieve arbitrary even-order accuracy in space and second-order accuracy in time.

CNOC schemes are uniquely solvable at each time step. In the practical computation, imaginary time grid points W_h^{-1} are used. W_h^{-1} can be eliminated by combining (2.23) and the third equality in (2.24). Choosing $n=0$ in (2.23), we can obtain W_h^1. Setting $n=0$ in (2.22), since W_h^0, W_h^1, Ψ_h^0 are known, we can solve for Ψ_h^1, and then obtain W_h^2 from (2.23), etc. Overall, only linear systems need to be solved at each time step.

Algorithm 2.1 Fully-discrete High-order OC Schemes

1: Find W_h^1 to satisfy the following equation by putting $n=0$ in (2.23):

$$\begin{aligned} &\delta_t^2 W_{j,k}^{0}-\frac{1}{2}\Big(C_\mu^x\big(W_{j,k}^{1}+W_{j,k}^{-1}\big)+C_\mu^y\big(W_{j,k}^{1}+W_{j,k}^{-1}\big)\Big)\\ &=C_\mu^x\big|\Psi_{j,k}^{0}\big|^2+C_\mu^y\big|\Psi_{j,k}^{0}\big|^2,\quad (j,k)\in\Theta_{JK}. \end{aligned}$$

2: Find Ψ_h^1 to satisfy the following equation by putting $n=0$ in (2.22):

$$\begin{aligned} &i\delta_t{}^{+}\Psi_{j,k}^{0}+\frac{1}{2}C_\mu^x\big(\Psi_{j,k}^{1}+\Psi_{j,k}^{0}\big)+\frac{1}{2}C_\mu^y\big(\Psi_{j,k}^{1}+\Psi_{j,k}^{0}\big)\\ &=\frac{1}{4}\big(W_{j,k}^{1}+W_{j,k}^{0}\big)\big(\Psi_{j,k}^{1}+\Psi_{j,k}^{0}\big),\quad (j,k)\in\Theta_{JK}. \end{aligned}$$

3: Find $W_h^2, \Psi_h^2, \ldots$ for $n\geq 1$.

For uniform grids, fast Fourier transform (FFT) can be utilized to solve the resulting linear systems. On the other hand, due to the large stencils of CNOC schemes with spatial

accuracy more than second-order, iterative method can be designed based on second-order OC schemes (block tridiagonal matrix). Since FFT based fast algorithms are easy to implement for the second order OC schemes, such simple iterative procedure could greatly reduce the computational cost and an iterative solver is presented in Appendix.

CNOC schemes also have two important conserved quantities.

Theorem 2.3. *Fully-discrete high-order OC schemes* (2.22)-(2.24) *maintain mass conservation, i.e.*

$$M_h^n := \left\|\Psi_h^n\right\|_H^2 = M_h^0, \quad n = 0, 1, \ldots, N.$$

Proof. Calculating the discrete inner product of (2.22) with $2\Psi_h^{n+1/2}$ and taking the imaginary part gives

$$\begin{aligned} &\operatorname{Im}\left\langle i\delta_t^+\Psi_h^n, 2\Psi_h^{n+1/2}\right\rangle_H + \frac{1}{2}\operatorname{Im}\left\langle C_\mu^x\left(\Psi_h^{n+1}+\Psi_h^n\right), 2\Psi_h^{n+1/2}\right\rangle_H \\ &\quad + \frac{1}{2}\operatorname{Im}\left\langle C_\mu^y\left(\Psi_h^{n+1}+\Psi_h^n\right), 2\Psi_h^{n+1/2}\right\rangle_H \\ &= \operatorname{Im}\left\langle W_h^{n+1/2}\Psi_h^{n+1/2}, 2\Psi_h^{n+1/2}\right\rangle_H, \end{aligned} \tag{2.25}$$

where

$$\operatorname{Im}\left\langle i\delta_t^+\Psi_h^n, 2\Psi_h^{n+1/2}\right\rangle_H = \operatorname{Re}\left\langle \delta_t^+\Psi_h^n, 2\Psi_h^{n+1/2}\right\rangle_H = \frac{1}{\tau}\left(\|\Psi_h^{n+1}\|_H^2 - \|\Psi_h^n\|_H^2\right), \tag{2.26}$$

$$\operatorname{Im}\left\langle C_\mu^x\left(\Psi_h^{n+1}+\Psi_h^n\right), 2\Psi_h^{n+1/2}\right\rangle_H = 0, \quad \operatorname{Im}\left\langle C_\mu^y\left(\Psi_h^{n+1}+\Psi_h^n\right), 2\Psi_h^{n+1/2}\right\rangle_H = 0, \tag{2.27}$$

$$\operatorname{Im}\left\langle W_h^{n+1/2}\Psi_h^{n+1/2}, 2\Psi_h^{n+1/2}\right\rangle_H = 0. \tag{2.28}$$

Substituting (2.26)-(2.28) into (2.25), we arrive at $\|\Psi_h^{n+1}\|_H^2 - \|\Psi_h^n\|_H^2 = 0$, and the conclusion follows. □

Define the discrete total energy

$$\begin{aligned} E_h^n = &\frac{1}{2}\left(\left\|\delta_x^+\Psi_h^{n+1}\right\|_B^2 + \left\|\delta_y^+\Psi_h^{n+1}\right\|_B^2 + \left\|\delta_x^+\Psi_h^n\right\|_B^2 + \left\|\delta_y^+\Psi_h^n\right\|_B^2\right) \\ &+ \frac{1}{2}\left(\left\|\delta_x^+u_h^{n+1/2}\right\|_B^2 + \left\|\delta_y^+u_h^{n+1/2}\right\|_B^2\right) + \frac{1}{4}\left(\left\|W_h^{n+1}\right\|_H^2 + \left\|W_h^n\right\|_H^2\right) \\ &+ \frac{1}{4}h_xh_y\sum_{j=0}^{J-1}\sum_{k=0}^{K-1}\left(W_{j,k}^{n+1}+W_{j,k}^n\right)\left(\left|\Psi_{j,k}^{n+1}\right|^2 + \left|\Psi_{j,k}^n\right|^2\right), \end{aligned}$$

where $u_h^{n+1/2}$ satisfying $\langle u_h^{n+1/2}, 1\rangle_H = 0$ is uniquely determined by (from the initialization $\langle \omega_h, 1\rangle = 0$)

$$C_\mu^x u_h^{n+1/2} + C_\mu^x u_h^{n+1/2} = \delta_t^+ W_h^n. \tag{2.29}$$

Then CNOC schemes (2.22)-(2.24) conserve the above energy.

Theorem 2.4. *Full-discrete high-order OC schemes* (2.22)-(2.24) *can maintain energy conservation — i.e.*

$$E_h^n = E_h^{n-1} = \cdots = E_h^0, \quad n = 1, 2, \ldots, N.$$

Proof. By calculating the discrete inner product of (2.22) with $\Psi_h^{n+1} - \Psi_h^n$ and then taking the real part yields

$$\begin{aligned} &\mathrm{Re}\left\langle i\delta_t^+\Psi_h^n, \Psi_h^{n+1} - \Psi_h^n\right\rangle_H + \mathrm{Re}\left\langle C_\mu^x \Psi_h^{n+1/2}, \Psi_h^{n+1} - \Psi_h^n\right\rangle_H \\ &\quad + \mathrm{Re}\left\langle C_\mu^y \Psi_h^{n+1/2}, \Psi_h^{n+1} - \Psi_h^n\right\rangle_H \\ &= \mathrm{Re}\left\langle W_h^{n+1/2}\Psi_h^{n+1/2}, \Psi_h^{n+1} - \Psi_h^n\right\rangle_H. \end{aligned} \tag{2.30}$$

From summation by parts, we have

$$\mathrm{Re}\left\langle i\delta_t^+\Psi_h^n, \Psi_h^{n+1} - \Psi_h^n\right\rangle_H = 0, \tag{2.31}$$

$$\mathrm{Re}\left\langle C_\mu^x \Psi_h^{n+1/2}, \Psi_h^{n+1} - \Psi_h^n\right\rangle_H = -\frac{1}{2}\left(\left\|\delta_x^+\Psi_h^{n+1}\right\|_B^2 - \left\|\delta_x^+\Psi_h^n\right\|_B^2\right), \tag{2.32}$$

$$\mathrm{Re}\left\langle C_\mu^y \Psi_h^{n+1/2}, \Psi_h^{n+1} - \Psi_h^n\right\rangle_H = -\frac{1}{2}\left(\left\|\delta_y^+\Psi_h^{n+1}\right\|_B^2 - \left\|\delta_y^+\Psi_h^n\right\|_B^2\right), \tag{2.33}$$

$$\begin{aligned} &\mathrm{Re}\left\langle W_h^{n+1/2}\Psi_h^{n+1/2}, \Psi_h^{n+1} - \Psi_h^n\right\rangle_H \\ &= \frac{1}{4}h_x h_y \sum_{j=0}^{J-1}\sum_{k=0}^{K-1}\left(W_{j,k}^{n+1} + W_{j,k}^n\right)\left(\left|\Psi_{j,k}^{n+1}\right|^2 - \left|\Psi_{j,k}^n\right|^2\right). \end{aligned} \tag{2.34}$$

Substituting (2.31)-(2.34) into (2.30), we arrive at

$$\begin{aligned} &\frac{1}{2}\left(\left\|\delta_x^+\Psi_h^{n+1}\right\|_B^2 + \left\|\delta_y^+\Psi_h^{n+1}\right\|_B^2 - \left\|\delta_x^+\Psi_h^n\right\|_B^2 - \left\|\delta_y^+\Psi_h^n\right\|_B^2\right) \\ &\quad + \frac{1}{4}\left\langle W_h^{n+1} + W_h^n, \left|\Psi_h^{n+1}\right|^2 - \left|\Psi_h^n\right|^2\right\rangle_H = 0. \end{aligned} \tag{2.35}$$

Taking the discrete inner product of (2.23) with $(\tau/2)(u_h^{n+1/2} + u_h^{n-1/2})$, we obtain

$$II_1 - II_2 - II_3 = 0, \tag{2.36}$$

where

$$\begin{aligned} II_1 &= \frac{\tau}{2}\left\langle \delta_t^2 W_h^n, u_h^{n+1/2} + u_h^{n-1/2}\right\rangle_H \\ &= \frac{\tau}{2}\left\langle \delta_t^-\left(C_\mu^x u_h^{n+1/2} + C_\mu^y u_h^{n+1/2}\right), u_h^{n+1/2} + u_h^{n-1/2}\right\rangle_H \\ &= -\frac{1}{2}\left(\left\|\delta_x^+ u_h^{n+1/2}\right\|_B^2 + \left\|\delta_y^+ u_h^{n+1/2}\right\|_B^2\right) \\ &\quad + \frac{1}{2}\left(\left\|\delta_x^+ u_h^{n-1/2}\right\|_B^2 + \left\|\delta_y^+ u_h^{n-1/2}\right\|_B^2\right), \\ II_2 &= \frac{\tau}{4}\left\langle C_\mu^x\left(W_h^{n+1} + W_h^{n-1}\right), u_h^{n+1/2} + u_h^{n-1/2}\right\rangle_H \end{aligned} \tag{2.37}$$

$$
\begin{aligned}
&+\frac{\tau}{4}\Big\langle C_\mu^y\big(W_h^{n+1}+W_h^{n-1}\big),u_h^{n+1/2}+u_h^{n-1/2}\Big\rangle_H\\
&=\frac{\tau}{4}\big\langle W_h^{n+1}+W_h^{n-1},\delta_t^+W_h^n+\delta_t^+W_h^{n-1}\big\rangle_H\\
&=\frac{1}{4}\Big(\big\|W_h^{n+1}\big\|_H^2-\big\|W_h^{n-1}\big\|_H^2\Big),
\end{aligned}\tag{2.38}
$$

$$
\begin{aligned}
II_3&=\frac{\tau}{2}\Big\langle C_\mu^x\big|\Psi_h^n\big|^2+C_\mu^y\big|\Psi_h^n\big|^2,u_h^{n+1/2}+u_h^{n-1/2}\Big\rangle_H\\
&=\frac{\tau}{2}\Big\langle\big|\Psi_h^n\big|^2,C_\mu^x\big(u_h^{n+1/2}+u_h^{n-1/2}\big)+C_\mu^y\big(u_h^{n+1/2}+u_h^{n-1/2}\big)\Big\rangle_H\\
&=\frac{\tau}{2}\Big\langle\big|\Psi_h^n\big|^2,\delta_t^+W_h^n+\delta_t^+W_h^{n-1}\Big\rangle_H\\
&=\frac{1}{2}\Big\langle\big|\Psi_h^n\big|^2,W_h^{n+1}-W_h^{n-1}\Big\rangle_H.
\end{aligned}\tag{2.39}
$$

Substituting (2.37)-(2.39) into (2.36), we arrive at

$$
\begin{aligned}
&\frac{1}{2}\Big(\big\|\delta_x^+u_h^{n+1/2}\big\|_B^2+\big\|\delta_y^+u_h^{n+1/2}\big\|_B^2\Big)-\frac{1}{2}\Big(\big\|\delta_x^+u_h^{n-1/2}\big\|_B^2+\Big\|\delta_y^+u_h^{n-1/2}\Big\|_B^2\Big)\\
&\quad+\frac{1}{4}\Big(\big\|W_h^{n+1}\big\|_H^2-\big\|W_h^{n-1}\big\|_H^2\Big)+\frac{1}{2}\Big\langle\big|\Psi_h^n\big|^2,W_h^{n+1}-W_h^{n-1}\Big\rangle_H=0.
\end{aligned}\tag{2.40}
$$

Summing (2.35) together for $n=n,n-1$, we get

$$
\begin{aligned}
&\frac{1}{2}\sum_{m=n,n+1}\Big(\big\|\delta_x^+\Psi_h^m\big\|_B^2+\big\|\delta_y^+\Psi_h^m\big\|_B^2\Big)-\frac{1}{2}\sum_{m=n-1,n}\Big(\big\|\delta_x^+\Psi_h^m\big\|_B^2+\big\|\delta_y^+\Psi_h^m\big\|_B^2\Big)\\
&\quad-\frac{1}{2}\Big\langle W_h^{n+1}-W_h^n,\big|\Psi_h^n\big|^2\Big\rangle_H+\frac{1}{4}\Big\langle W_h^{n+1}+W_h^n,\big|\Psi_h^{n+1}\big|^2+\big|\Psi_h^n\big|^2\Big\rangle_H\\
&\quad-\frac{1}{4}\Big\langle W_h^n+W_h^{n-1},\big|\Psi_h^n\big|^2-\big|\Psi_h^{n-1}\big|^2\Big\rangle_H=0.
\end{aligned}\tag{2.41}
$$

Summing (2.40) and (2.41), we have $E_h^n=E_h^{n-1}$, and the conclusion follows. □

Remark 2.1. According to Theorems 2.3 and 2.4, fully-discrete high-order OC schemes (2.22)-(2.24) are unconditionally stable.

Remark 2.2. For periodic problems (2.1)-(2.3), the conserved quantities are obtained by CNOC schemes (2.22)-(2.24) which can achieve spectral-order accuracy whether it is a low-order CNOC scheme or a high-order CNOC scheme (trapezoidal rule for integrating periodic functions is spectrally accurate), numerical experiments will verify this result in the next section. For related discussion, readers can refer to [17].

3. Numerical Results

In this section, numerical results are presented to validate the theoretical analysis. When the iterative solver (see Appendix) is used to compute the linear systems in CNOC

schemes, the error threshold is set to 10^{-12}, i.e. when the maximum error of two consecutive iterates satisfies

$$\max_{j,k\in\Theta_{JK}} \left|\Psi_{j,k}^{n+1,m+1}-\Psi_{j,k}^{n+1,m}\right| < 10^{-12},$$
$$\max_{j,k\in\Theta_{JK}} \left|W_{j,k}^{n+1,m+1}-W_{j,k}^{n+1,m}\right| < 10^{-12},$$

we set

$$\Psi_{j,k}^{n+1}=\Psi_{j,k}^{n+1,m+1}, \quad W_{j,k}^{n+1}=W_{j,k}^{n+1,m+1},$$

and the iteration is terminated.

In numerical experiments, uniform mesh size is adopted and $h_x = h_y = h$ in the two dimensional case. Let $\Psi(\cdot,t_n)$, $W(\cdot,t_n)$ be the exact solutions, $\Psi_{h,\tau}^n$, $W_{h,\tau}^n$ be the numerical solutions of (2.22)-(2.24) generated by a numerical method with mesh size h and time step τ. The grid error functions are

$$e_{h,\tau}(t_n) := \Psi(\cdot,t_n)-\Psi_{h,\tau}^n, \quad \theta_{h,\tau}(t_n) := W(\cdot,t_n)-W_{h,\tau}^n.$$

The maximum norm errors are

$$\xi_{h,\tau}(T) = \max_{0\le n\le N=T/\tau} \left\{\|e_{h,\tau}(t_n)\|_\infty, \|\theta_{h,\tau}(t_n)\|_\infty\right\},$$

and the spatial accuracy order is computed by

$$\text{order}_{\text{space}} = \frac{\ln(\xi_{h_1,\tau_e}/\xi_{h_2,\tau_e})}{\ln(h_1/h_2)}$$

for a very small time step size τ_e. The temporal accuracy order is defined for a very fine mesh size h_e as

$$\text{order}_{\text{time}} = \frac{\ln(\xi_{h_e,\tau_1}/\xi_{h_e,\tau_2})}{\ln(\tau_1/\tau_2)}$$

and the mass error is defined as

$$\text{error}_{\text{mass}} = \max_{0\le n\le N=T/\tau} \left|M(t_n)-M_h^n\right|.$$

Example 3.1. We choose a one dimensional computational domain $\Omega = [-20,20]$ and $t\in[0,6]$. The initial conditions for ZS (1.1)-(1.3) are taken as

$$\Psi(x,0)=\frac{\sqrt{6}}{2}\operatorname{sech} x e^{ix/4}, \quad W(x,0)=-2\operatorname{sech}^2 x, \quad W_t(x,0)=-2\operatorname{sech}^2 x\tanh x, \quad x\in\Omega.$$

We note that this is a soliton solution.

The spatial convergence order is displayed in Table 1, where a very small time step size $\tau_e = 10^{-5}$ is used to make the temporal discretization error negligible. From Table 1, spatial orders of CNOC4 and CNOC6 schemes are found to be $\mathcal{O}(h^4)$ and $\mathcal{O}(h^6)$, respectively. The temporal convergence order is shown in Table 2, where a very fine mesh size $h = 0.01$

is adopted. The temporal accuracy is found to be $\mathcal{O}(\tau^2)$. Table 3 depicts the conserved quantities of CNOC schemes, which can achieve spectral-order accuracy whether it is a low-order CNOC scheme or a high-order CNOC scheme. We verify the conservation properties of CNOC6 and simulate its dynamic behavior. Fig. 1 presents the evolution of the discrete mass and the discrete total energy and its components over time — i.e.

$$\begin{aligned}
\mathrm{Epk}_h^n &= \frac{1}{2}\left(\left\|\delta_x^+\Psi_h^{n+1}\right\|_B^2 + \left\|\delta_y^+\Psi_h^{n+1}\right\|_B^2 + \left\|\delta_x^+\Psi_h^{n}\right\|_B^2 + \left\|\delta_y^+\Psi_h^{n}\right\|_B^2\right),\\
\mathrm{Ewk}_h^n &= \frac{1}{2}\left(\left\|\delta_x^+u_h^{n+1/2}\right\|_B^2 + \left\|\delta_y^+u_h^{n+1/2}\right\|_B^2\right),\\
\mathrm{Ewpot}_h^n &= \frac{1}{4}\left(\left\|W_h^{n+1}\right\|_H^2 + \left\|W_h^{n}\right\|_H^2\right),\\
\mathrm{Einter}_h^n &= \frac{1}{4}h_xh_y\sum_{j=0}^{J-1}\sum_{k=0}^{K-1}(W_{j,k}^{n+1}+W_{j,k}^{n})\left(\left|\Psi_{j,k}^{n+1}\right|^2 + \left|\Psi_{j,k}^{n}\right|^2\right).
\end{aligned}$$

Plots for $|\Psi|$ and W are given in Fig. 2 with $h = 0.1$ and $\tau = 0.01$ at time $T = 2, 4, 6$, where the soliton dynamics is clearly observed.

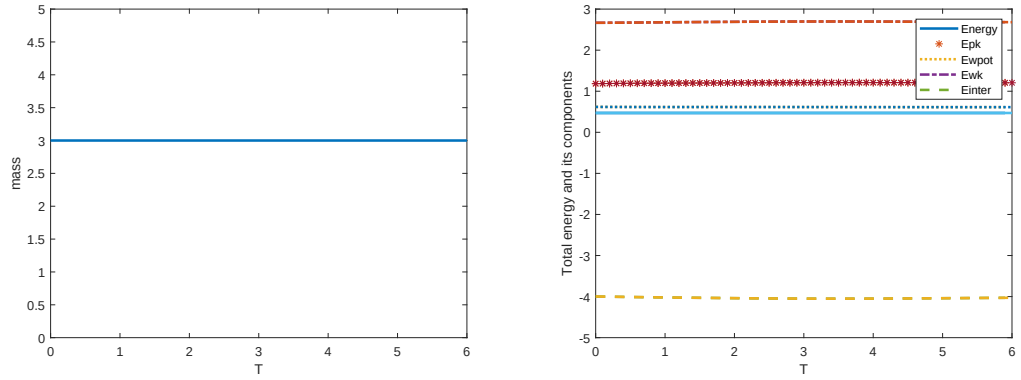

Figure 1: Example 3.1: Discrete mass (left) and discrete total energy and its components (right).

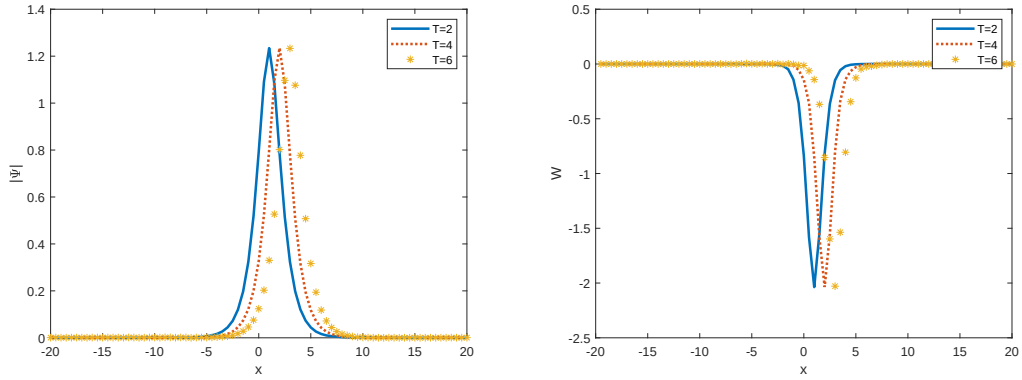

Figure 2: Example 3.1: $|\Psi|$ (left) and W (right) at time $T = 2, 4, 6$.

Table 1: Example 3.1: Spatial accuracy orders with $\tau = 10^{-5}$ at time $T = 1$ under different mesh size h.

Schemes	h	$\xi_{h,\tau}(T=1)$	$\text{Order}_{\text{space}}$
CNOC4	0.4	1.0725E-02	*
	0.2	7.2368E-04	3.8895
	0.1	4.6675E-05	3.9546
	0.05	2.9830E-06	3.9678
CNOC6	0.4	3.3514E-03	*
	0.2	6.7629E-05	5.6309
	0.1	1.1018E-06	5.8143
	0.05	1.7492E-08	5.9770

Table 2: Example 3.1: Temporal accuracy orders with $h = 0.01$ at time $T = 1$ under different time step τ.

Schemes	τ	$\xi_{h,\tau}(T=1)$	$\text{Order}_{\text{time}}$
CNOC4	0.04	1.2342E-03	*
	0.02	3.0853E-04	2.0001
	0.01	7.7131E-05	2.0000
	0.005	1.9286E-05	1.9997
CNOC6	0.04	1.2342E-03	*
	0.02	3.0852E-04	2.0001
	0.01	7.7127E-05	2.0000
	0.005	1.9282E-05	2.0000

Table 3: Example 3.1: Mass error with $\tau = 0.01$ at time $T = 1$ under different time step h.

Schemes	h	$\text{Error}_{\text{mass}}$
CNOC4	0.4	3.0161E-00
	0.2	4.3210E-01
	0.1	6.1265E-03
	0.05	6.3370E-07
CNOC6	0.4	2.7504E-00
	0.2	3.9304E-01
	0.1	5.6587E-03
	0.05	5.8531E-07

Example 3.2. We choose a one dimensional computational domain $\Omega = [-\pi, \pi]$ and $t \in [0, 6]$. The initial conditions for ZS (1.1)-(1.3) are taken as

$$\Psi(x,0) = \sin(x), \quad W(x,0) = \sin^2(x), \quad W_t(x,0) = 0.$$

The spatial accuracy is displayed in Table 4 with a sufficiently small time step size $\tau = 10^{-5}$, and the spatial convergence orders of CNOC4 and CNOC6 schemes are found to be $\mathcal{O}(h^4)$ and $\mathcal{O}(h^6)$, respectively. The temporal accuracy order is displayed in Table 5, where a very small mesh size $h = 0.01$ is used. The temporal accuracy is clear at $\mathcal{O}(\tau^2)$. Table 6 shows the mass of the numerical solution is very close to the mass of the exact solution for $\tau = 0.01$ at time $T = 1$. Indeed, the mass errors of CNOC4 and CNOC6 schemes achieve spectral-order accuracy. Fig. 3 shows the evolution of the discrete mass and the discrete total energy with its components over time. Densities $|\Psi|^2$ and W are shown in Fig. 4 to demonstrate the dynamical evolution of ZS ($h = 0.1$, $\tau = 0.01$).

Table 4: Example 3.2: Spatial accuracy orders with $\tau = 10^{-5}$ at time $T = 1$ under different mesh size h.

Schemes	h	$\xi_{h,\tau}(T=1)$	$\text{Order}_{\text{space}}$
CNOC4	0.4	8.1614E-03	*
	0.2	6.3953E-04	3.6737
	0.1	4.2878E-05	3.8987
	0.05	2.8073E-06	3.9678
CNOC6	0.4	1.8335E-03	*
	0.2	4.9074E-05	5.2235
	0.1	8.6480E-06	5.8265
	0.05	2.2405E-08	5.2705

Table 5: Example 3.2: Temporal accuracy orders with $h = 0.01$ at time $T = 1$ under different time step τ.

Schemes	τ	$\xi_{h,\tau}(T=1)$	$\text{Order}_{\text{time}}$
CNOC4	0.04	2.8092E-02	*
	0.02	8.2976E-03	1.6928
	0.01	2.0907E-03	1.9887
	0.005	5.2250E-04	2.0005
CNOC6	0.04	2.1746E-02	*
	0.02	8.2976E-03	1.3900
	0.01	2.0907E-03	1.9887
	0.005	5.2250E-05	2.0005

Table 6: Example 3.2: Mass errors with $\tau = 0.01$ at time $T = 1$ under different time step h.

Schemes	h	$\text{Error}_{\text{mass}}$
CNOC4	$\pi/2$	8.2156E-12
	$\pi/4$	1.0658E-12
	$\pi/8$	3.5527E-13
	$\pi/16$	4.4490E-13
CNOC6	$\pi/2$	7.1054E-13
	$\pi/4$	3.5527E-13
	$\pi/8$	2.6645E-13
	$\pi/16$	2.6645E-13

Example 3.3. We choose a two dimensional computational domain $\Omega = [-20, 20]^2$ and $t \in [0, 4]$. The initial conditions for ZS (1.1)-(1.3) are taken as

$$\Psi(x, y, 0) = \frac{1}{\sqrt{\pi}} \exp\left(-\frac{x^2 + y^2}{2}\right), \quad W(x, y, 0) = -\sqrt{\pi} \exp\left(-\frac{x^2 + y^2}{2}\right),$$
$$W_t(x, y, 0) = 0, \quad (x, y) \in \Omega.$$

Fig. 5 shows the evolution of the discrete mass and the discrete total energy and its components over time with $h_x = h_y = 0.5$, $\tau = 0.1$. In Figs. 6-9, time evolutions of $|\Psi|^2$ and W are presented with $h_x = h_y = 0.5$, $\tau = 0.1$. Dynamical changes in the peaks and surface plots of $|\Psi|^2$ and W can be observed.

4. Conclusion

In this work we constructed conservative high-order OC schemes for solving ZS. Semi-discrete-in-space high-order OC schemes were obtained by applying the OC method to spatial discretization. These schemes can maintain mass conservation and energy conservation. By applying CN technology for temporal discretization, CNOC schemes were derived

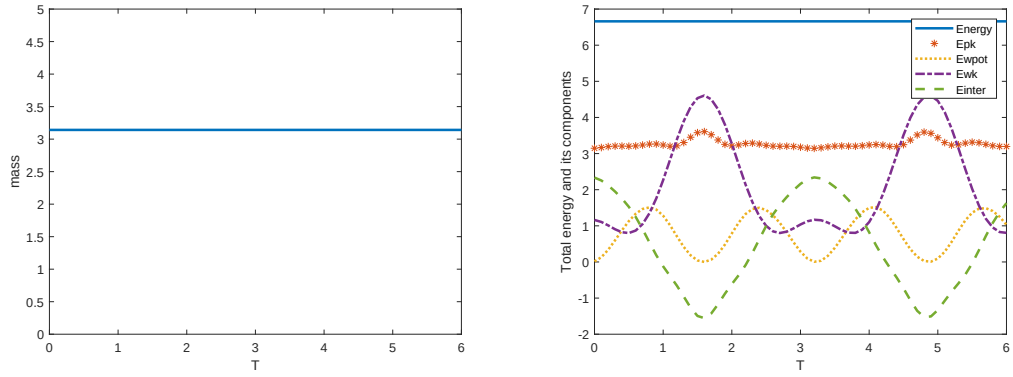

Figure 3: Example 3.2: Discrete mass (left) and discrete total energy and its components (right).

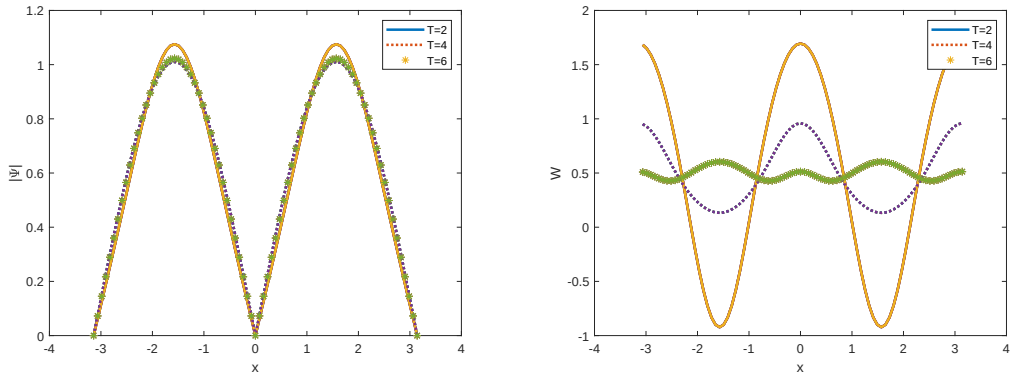

Figure 4: Example 3.2: $|\Psi|$ (left) and W (right) at time $T = 2, 4, 6$.

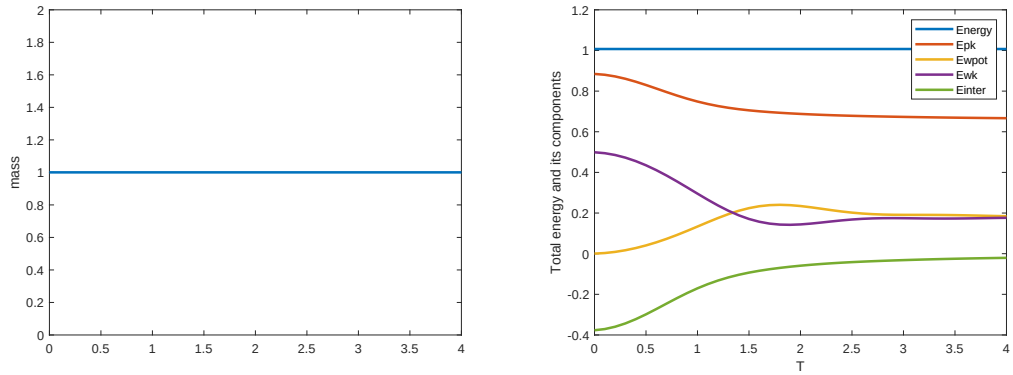

Figure 5: Example 3.3: Discrete mass (left) and discrete total energy and its components (right).

and keep maintain mass conservation and energy conservation at the discrete level. The temporal accuracy of those schemes are second order, and the spatial accuracy can achieve arbitrary even order. Numerical experiments confirmed the accuracy order and the conservation properties, and demonstrated the dynamic evolution.

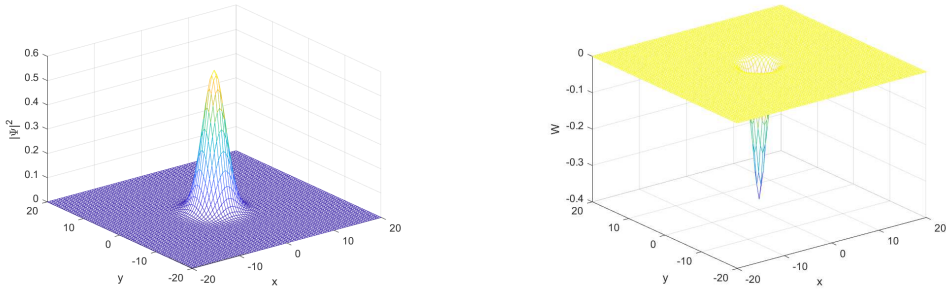

Figure 6: Example 3.3: $|\Psi|$ (left) and W (right) at time $T = 1$.

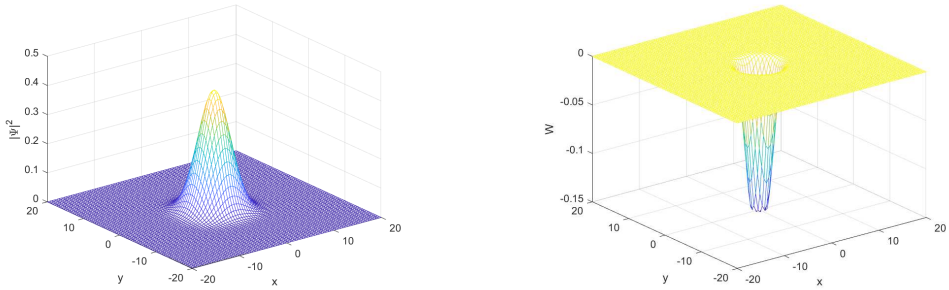

Figure 7: Example 3.3: $|\Psi|$ (left) and W (right) at time $T = 1.5$.

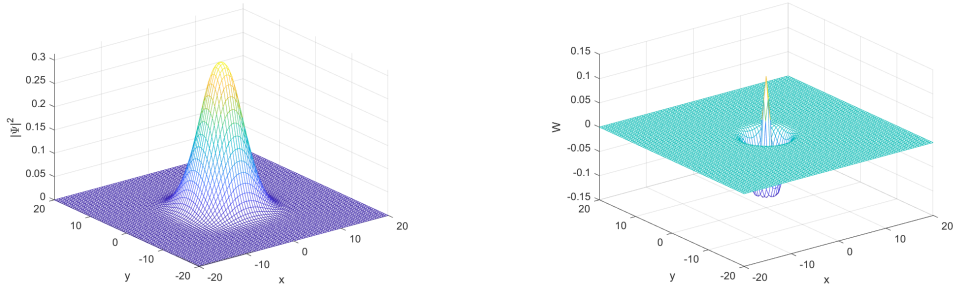

Figure 8: Example 3.3: $|\Psi|$ (left) and W (right) at time $T = 2$.

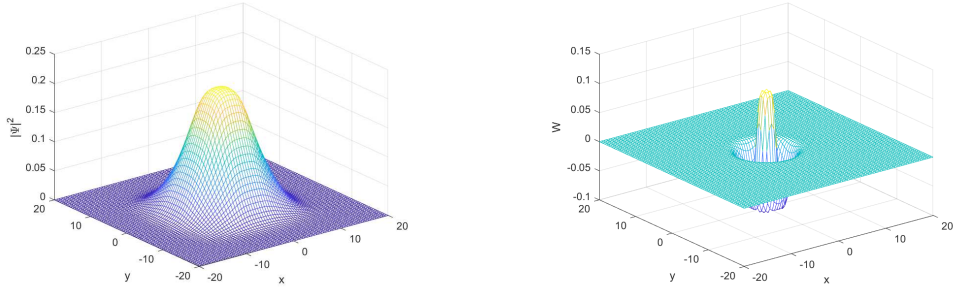

Figure 9: Example 3.3: $|\Psi|$ (left) and W (right) at time $T = 3$.

Appendix

The proposed iterative algorithm for the CNOC4 scheme is given as follows. To simplify the expression, we set that $h_x = h_y = h$. Letting $n = 0$ in (2.23), combining with the third equation in (2.24), we have

$$\omega(x_j, y_k) = \frac{1}{2\tau}\big(W^1_{j,k} - W^{-1}_{j,k}\big),$$
$$\delta_t^2 W^0_{j,k} - \frac{1}{2}\Big(C_1^x\big(W^1_{j,k} + W^{-1}_{j,k}\big) + C_1^y\big(W^1_{j,k} + W^{-1}_{j,k}\big)\Big) = C_1^x\big|\Psi^0_{j,k}\big|^2 + C_1^y\big|\Psi^0_{j,k}\big|^2.$$

W^1_h can be obtained by eliminating W^{-1}_h. Letting $\tau/h = \lambda$, we can get

$$\begin{aligned}
&\frac{1}{12}\lambda^2 W^1_{j+2,k} - \frac{4}{3}\lambda^2 W^1_{j+1,k} + (2+5\lambda^2)W^1_{j,k} - \frac{4}{3}\lambda^2 W^1_{j-1,k} + \frac{1}{12}\lambda^2 W^1_{j-2,k} \\
&\quad + \frac{1}{12}\lambda^2 W^1_{j,k+2} - \frac{4}{3}\lambda^2 W^1_{j,k+1} - \frac{4}{3}\lambda^2 W^1_{j,k-1} + \frac{1}{12}\lambda^2 W^1_{j,k-2} \\
&= \tau^2\Big(C_1^x\Big(\big|\Psi^0_{j,k}\big|^2\Big) + C_1^y\Big(\big|\Psi^0_{j,k}\big|^2\Big)\Big) + 2W^0_{j,k} + 2\tau\omega(x_j, y_k) \\
&\quad - \tau^3\big(C_1^x\omega(x_j, y_k) + C_1^y\omega(x_j, y_k)\big).
\end{aligned} \tag{4.1}$$

Further, the Eq. (4.1) can be written as

$$S_2 D^1_{k-2} + S_1 D^1_{k-1} + \bar{S} D^1_k + S_1 D^1_{k+1} + S_2 D^1_{k+2} = O_k,$$

i.e.

$$\begin{bmatrix}
\bar{S} & S_1 & S_2 & & & & & \\
S_1 & \bar{S} & S_1 & S_2 & & & & \\
S_2 & S_1 & \bar{S} & S_1 & S_2 & & & \\
 & \ddots & \ddots & \ddots & \ddots & \ddots & & \\
 & & \ddots & \ddots & \ddots & \ddots & \ddots & \\
 & & & S_2 & S_1 & \bar{S} & S_1 & S_2 \\
 & & & & S_2 & S_1 & \bar{S} & S_1 \\
 & & & & & S_2 & S_1 & \bar{S}
\end{bmatrix}_{K\times K}
\begin{bmatrix} D^1_1 \\ D^1_2 \\ \vdots \\ \vdots \\ \vdots \\ \vdots \\ D^1_{K-1} \\ D^1_K \end{bmatrix}
=
\begin{bmatrix} O_1 \\ O_2 \\ \vdots \\ \vdots \\ \vdots \\ \vdots \\ O_{K-1} \\ O_K \end{bmatrix},$$

where for $k = 1, 2, \ldots, K$,

$$\begin{aligned}
O_k &= \big(\gamma_{1,k}, \gamma_{2,k}, \cdots, \gamma_{J,k}\big)^\top, \\
D^1_k &= \Big(W^1_{1,k}, W^1_{2,k}, \cdots, W^1_{J,k}\Big)^\top, \\
\gamma_{j,k} &= \tau^2\Big(C_1^x\Big(\big|\Psi^0_{j,k}\big|^2\Big) + C_1^y\Big(\big|\Psi^0_{j,k}\big|^2\Big)\Big) \\
&\quad + 2W^0_{j,k} + 2\tau\omega(x_j, y_k) \\
&\quad - \tau^3\big(C_1^x\omega(x_j, y_k) + C_1^y\omega(x_j, y_k)\big).
\end{aligned}$$

The block matrices are

$$S_1 = -\frac{4}{3}\lambda^2 I_{J\times J}, \quad S_2 = \frac{1}{12}\lambda^2 I_{J\times J}, \quad \bar{S} = 2\bar{A},$$

where

$$\bar{A} = \begin{bmatrix} 1+\frac{5}{2}\lambda^2 & -\frac{2}{3}\lambda^2 & \frac{1}{24}\lambda^2 & 0 & \cdots & 0 & \frac{1}{24}\lambda^2 & -\frac{2}{3}\lambda^2 \\ -\frac{2}{3}\lambda^2 & 1+\frac{5}{2}\lambda^2 & -\frac{2}{3}\lambda^2 & \frac{1}{24}\lambda^2 & 0 & \cdots & 0 & \frac{1}{24}\lambda^2 \\ \frac{1}{24}\lambda^2 & -\frac{2}{3}\lambda^2 & 1+\frac{5}{2}\lambda^2 & -\frac{2}{3}\lambda^2 & \frac{1}{24}\lambda^2 & 0 & \cdots & 0 \\ 0 & \ddots & \ddots & \ddots & \ddots & \ddots & 0 & \vdots \\ \vdots & 0 & \ddots & \ddots & \ddots & \ddots & \ddots & 0 \\ 0 & \vdots & 0 & \frac{1}{24}\lambda^2 & -\frac{2}{3}\lambda^2 & 1+\frac{5}{2}\lambda^2 & -\frac{2}{3}\lambda^2 & \frac{1}{24}\lambda^2 \\ \frac{1}{24}\lambda^2 & 0 & \vdots & 0 & \ddots & -\frac{2}{3}\lambda^2 & 1+\frac{5}{2}\lambda^2 & -\frac{2}{3}\lambda^2 \\ -\frac{2}{3}\lambda^2 & \frac{1}{24}\lambda^2 & 0 & \cdots & 0 & \frac{1}{24}\lambda^2 & -\frac{2}{3}\lambda^2 & 1+\frac{5}{2}\lambda^2 \end{bmatrix}_{J\times J}.$$

In the process of solving W_h^1, since solving the linear algebraic equation (4.1) of the block five diagonal matrix requires a large amount of computation, the high-order term is iteratively calculated. The Eq. (4.1) can be written in the following iterative schemes:

$$\begin{aligned} &\frac{1}{12}\lambda^2 W_{j+2,k}^{1,m+1} - \frac{4}{3}\lambda^2 W_{j+1,k}^{1,m+1} + (2+5\lambda^2) W_{j,k}^{1,m+1} - \frac{4}{3}\lambda^2 W_{j-1,k}^{1,m+1} + \frac{1}{12}\lambda^2 W_{j-2,k}^{1,m+1} \\ &\quad + \frac{1}{12}\lambda^2 W_{j,k+2}^{1,m} - \frac{4}{3}\lambda^2 W_{j,k+1}^{1,m+1} - \frac{4}{3}\lambda^2 W_{j,k-1}^{1,m+1} + \frac{1}{12}\lambda^2 W_{j,k-2}^{1,m} \\ &= \tau^2 \left(C_1^x \left(\left| \Psi_{j,k}^0 \right|^2 \right) + C_1^y \left(\left| \Psi_{j,k}^0 \right|^2 \right) \right) + 2W_{j,k}^0 + 2\tau\omega(x_j, y_k) \\ &\quad - \tau^3 \left(C_1^x \omega(x_j, y_k) + C_1^y \omega(x_j, y_k) \right). \end{aligned} \tag{4.2}$$

Further, the Eq. (4.2) can be written as

$$S_2 D_{k-2}^{1,m} + S_1 D_{k-1}^{1,m+1} + \bar{S} D_k^{1,m+1} + S_1 D_{k+1}^{1,m+1} + S_2 D_{k+2}^{1,m} = O_k,$$

i.e.

$$\begin{bmatrix} \bar{S} & S_1 & & & & & & \\ S_1 & \bar{S} & S_1 & & & & & \\ & S_1 & \bar{S} & S_1 & & & & \\ & & \ddots & \ddots & \ddots & & & \\ & & & \ddots & \ddots & \ddots & & \\ & & & & S_1 & \bar{S} & S_1 & \\ & & & & & S_1 & \bar{S} & S_1 \\ & & & & & & S_1 & \bar{S} \end{bmatrix}_{K\times K} \begin{bmatrix} D_1^{1,m+1} \\ D_2^{1,m+1} \\ D_3^{1,m+1} \\ \vdots \\ \vdots \\ D_{K-2}^{1,m+1} \\ D_{K-1}^{1,m+1} \\ D_K^{1,m+1} \end{bmatrix} = \begin{bmatrix} O_1 - S_2 D_3^{1,m} \\ O_2 - S_2 D_4^{1,m} \\ O_3 - S_2 D_1^{1,m} - S_2 D_5^{1,m} \\ \vdots \\ \vdots \\ O_{K-2} - S_2 D_{K-4}^{1,m} - S_2 D_K^{1,m} \\ O_{K-1} - S_2 D_{K-3}^{1,m} \\ O_K - S_2 D_{K-2}^{1,m} \end{bmatrix}.$$

If $m=0$, then

$$D_k^{1,m}=\left(W_{1,k}^{1,m},W_{2,k}^{1,m},\cdots,W_{J,k}^{1,m}\right)^{\top}=\left(W_{1,k}^{0},W_{2,k}^{0},\cdots,W_{J,k}^{0}\right)^{\top}.$$

W_h^1 can be obtained by numerical iterative calculation when the iterative error is smaller than the given threshold.

Multiplying both sides of (2.21) by τ and let $\tau/h^2=\beta$, we get

$$\begin{aligned}&\frac{1}{12}\lambda^2W_{j+2,k}^{1,m+1}-\frac{4}{3}\lambda^2W_{j+1,k}^{1,m+1}+(2+5\lambda^2)W_{j,k}^{1,m+1}-\frac{4}{3}\lambda^2W_{j-1,k}^{1,m+1}\\&\quad+\frac{1}{12}\lambda^2W_{j-2,k}^{1,m+1}-\frac{1}{24}\beta\Psi_{j,k+2}^{n+1}+\frac{2}{3}\beta\Psi_{j,k+1}^{n+1}+\frac{2}{3}\beta\Psi_{j,k-1}^{n+1}-\frac{1}{24}\beta\Psi_{j,k-2}^{n+1}\\&=\frac{\tau}{4}\left(W_{j,k}^{n+1}+W_{j,k}^{n}\right)\Psi_{j,k}^{n}+i\Psi_{j,k}^{n}-\frac{\tau}{2}\left(C_1^x\Psi_{j,k}^{n}+C_1^y\Psi_{j,k}^{n}\right).\end{aligned}\tag{4.3}$$

Further, the Eq. (4.3) can be written as

$$\Lambda_2Z_{k-2}^{n+1}+\Lambda_1Z_{k-1}^{n+1}+\Lambda Z_k^{n+1}+\Lambda_1Z_{k+1}^{n+1}+\Lambda_2Z_{k+2}^{n+1}=H_k,$$

i.e.

$$\begin{bmatrix}\Lambda&\Lambda_1&\Lambda_2&&&&&&\\\Lambda_1&\Lambda&\Lambda_1&\Lambda_2&&&&&\\\Lambda_2&\Lambda_1&\Lambda&\Lambda_1&\Lambda_2&&&&\\&\ddots&\ddots&\ddots&\ddots&\ddots&&&\\&&\ddots&\ddots&\ddots&\ddots&\ddots&&\\&&&\Lambda_2&\Lambda_1&\Lambda&\Lambda_1&\Lambda_2&\\&&&&\Lambda_2&\Lambda_1&\Lambda&\Lambda_1&\\&&&&&\Lambda_2&\Lambda_1&\Lambda&\end{bmatrix}_{K\times K}\begin{bmatrix}Z_1^{n+1}\\Z_2^{n+1}\\\vdots\\\vdots\\\vdots\\\vdots\\Z_{K-1}^{n+1}\\Z_K^{n+1}\end{bmatrix}=\begin{bmatrix}H_1\\H_2\\\vdots\\\vdots\\\vdots\\\vdots\\H_{K-1}\\H_K\end{bmatrix},$$

where for $k=1,2,\ldots,K$,

$$\begin{aligned}H_k&=(\vartheta_{1,k},\vartheta_{2,k},\cdots,\vartheta_{J,k})^{\top},\\Z_k^n&=(\Psi_{1,k}^n,\Psi_{2,k}^n,\cdots,\Psi_{J,k}^n)^{\top},\\\vartheta_{j,k}&=\frac{\tau}{4}\left(W_{j,k}^{n+1}+W_{j,k}^{n}\right)\Psi_{j,k}^{n}+i\Psi_{j,k}^{n}\\&\quad-\frac{\tau}{2}\left(C_1^x\Psi_{j,k}^{n}+C_1^y\Psi_{j,k}^{n}\right).\end{aligned}$$

The block matrices are

$$\Lambda_1=\frac{2}{3}\beta I_{J\times J},\quad \Lambda_2=-\frac{1}{24}\beta I_{J\times J},$$

$$\Lambda=\begin{bmatrix}
\bar{\Lambda}_{j,k} & \frac{2}{3}\beta & -\frac{1}{24}\beta & 0 & \cdots & 0 & -\frac{1}{24}\beta & \frac{2}{3}\beta \\
\frac{2}{3}\beta & \bar{\Lambda}_{j,k} & \frac{2}{3}\beta & -\frac{1}{24}\beta & 0 & \cdots & 0 & -\frac{1}{24}\beta \\
-\frac{1}{24}\beta & \frac{2}{3}\beta & \bar{\Lambda}_{j,k} & \frac{2}{3}\beta & -\frac{1}{24}\beta & 0 & \cdots & 0 \\
0 & \ddots & \ddots & \ddots & \ddots & \ddots & 0 & \vdots \\
\vdots & 0 & \ddots & \ddots & \ddots & \ddots & \ddots & 0 \\
0 & \vdots & 0 & -\frac{1}{24}\beta & \frac{2}{3}\beta & \bar{\Lambda}_{j,k} & \frac{2}{3}\beta & -\frac{1}{24}\beta \\
-\frac{1}{24}\beta & 0 & \vdots & 0 & \ddots & \frac{2}{3}\beta & \bar{\Lambda}_{j,k} & \frac{2}{3}\beta \\
\frac{2}{3}\beta & -\frac{1}{24}\beta & 0 & \cdots & 0 & -\frac{1}{24}\beta & \frac{2}{3}\beta & \bar{\Lambda}_{j,k}
\end{bmatrix}_{J\times J},$$

where

$$\bar{\Lambda}_{j,k}=i-\frac{5}{2}\beta-\frac{\tau}{4}\left(W_{j,k}^{n}+W_{j,k}^{n+1}\right)$$

in the block matrix Λ. Similar to (4.2), the linear algebraic equation (4.3) of block-five diagonal matrix can be solved by the iterative method. If $m=0$, then

$$Z_k^{n+1,m}=\left(\Psi_{1,k}^{n+1,m},\Psi_{2,k}^{n+1,m},\cdots,\Psi_{J,k}^{n+1,m}\right)^{\top}=\left(\Psi_{1,k}^{n},\Psi_{2,k}^{n},\cdots,\Psi_{J,k}^{n}\right)^{\top}.$$

The numerical solution Ψ_h^{n+1} can be obtained.

Multiplying both sides of (2.23) by τ^2, we get

$$\begin{aligned}
&\frac{1}{24}\lambda^2W_{j+2,k}^{n+1}-\frac{2}{3}\lambda^2W_{j+1,k}^{n+1}+\left(1+\frac{5}{2}\lambda^2\right)W_{j,k}^{n+1}-\frac{2}{3}\lambda^2W_{j-1,k}^{n+1}+\frac{1}{24}\lambda^2W_{j-2,k}^{n+1}\\
&\quad+\frac{1}{24}\lambda^2W_{j,k+2}^{n+1}-\frac{2}{3}\lambda^2W_{j,k+1}^{n+1}-\frac{2}{3}\lambda^2W_{j,k-1}^{n+1}+\frac{1}{24}\lambda^2W_{j,k-2}^{n+1}\\
&=2W_{j,k}^{n}-W_{j,k}^{n-1}+\tau^2\left(C_1^x\left(\left|\Psi_{j,k}^{n}\right|^2\right)+C_1^y\left(\left|\Psi_{j,k}^{n}\right|^2\right)\right)+\frac{\tau^2}{2}\left(C_1^xW_{j,k}^{n-1}+C_1^yW_{j,k}^{n-1}\right).
\end{aligned}\tag{4.4}$$

The Eq. (4.4) can be written as

$$A_2D_{k-2}^{n+1}+A_1D_{k-1}^{n+1}+\bar{A}D_k^{n+1}+A_1D_{k+1}^{n+1}+A_2D_{k+2}^{n+1}=F_k,$$

i.e.

$$\begin{bmatrix}
\bar{A} & A_1 & A_2 & & & & & \\
A_1 & \bar{A} & A_1 & A_2 & & & & \\
A_2 & A_1 & \bar{A} & A_1 & A_2 & & & \\
 & \ddots & \ddots & \ddots & \ddots & \ddots & & \\
 & & \ddots & \ddots & \ddots & \ddots & \ddots & \\
 & & & A_2 & A_1 & \bar{A} & A_1 & A_2 \\
 & & & & A_2 & A_1 & \bar{A} & A_1 \\
 & & & & & A_2 & A_1 & \bar{A}
\end{bmatrix}_{K\times K}\begin{bmatrix}D_1^{n+1}\\D_2^{n+1}\\\vdots\\\vdots\\\vdots\\\vdots\\D_{K-1}^{n+1}\\D_K^{n+1}\end{bmatrix}=\begin{bmatrix}F_1\\F_2\\\vdots\\\vdots\\\vdots\\\vdots\\F_{K-1}\\F_K\end{bmatrix},$$

where for $k = 1, 2, \ldots, K$,

$$\begin{aligned}
&F_k = (\varsigma_{1,k}, \varsigma_{2,k}, \cdots, \varsigma_{J,k})^\top,\\
&D_k^n = \left(W_{1,k}^n, W_{2,k}^n, \cdots, W_{J,k}^n\right)^\top,\\
&\varsigma_{j,k} = 2W_{j,k}^n - W_{j,k}^{n-1} + \tau^2\left(C_1^x\left(\left|\Psi_{j,k}^n\right|^2\right) + C_1^y\left(\left|\Psi_{j,k}^n\right|^2\right)\right)\\
&\qquad + \frac{\tau^2}{2}\left(C_1^x W_{j,k}^{n-1} + C_1^y W_{j,k}^{n-1}\right).
\end{aligned}$$

The block matrices are $A_1 = -(2/3)\lambda^2 I_{J\times J}$, $A_2 = (1/24)\lambda^2 I_{J\times J}$. Similar to (4.2), the linear algebraic equation (4.4) of the block five diagonal matrix can be solved by the iterative method. If $m = 0$, then

$$D_k^{n+1,m} = \left(W_{1,k}^{n+1,m}, W_{2,k}^{n+1,m}, \cdots, W_{J,k}^{n+1,m}\right)^\top = \left(W_{1,k}^n, W_{2,k}^n, \cdots, W_{J,k}^n\right)^\top.$$

The numerical solution W_h^{n+1} can be obtained accordingly.

Acknowledgements

X.-G. Li was supported by the National Natural Science Foundation of China (Grant No. 12272059). Y. Cai was partially supported by the National Natural Science Foundation of China (Grants Nos. 12171041, 11771036).

References

[1] H. Added and S. Added, *Equations of Langmuir turbulence and nonlinear Schrödinger equation: Smoothness and approximation*, J. Funct. Anal. **79**, 183–210 (1988).

[2] W. Bao and C. Su, *Uniform error bounds of a finite difference method for the Zakharov system in the subsonic limit regime via an asymptotic consistent formulation*, Multiscale Model. Simul. **15(2)**, 977–1002 (2017).

[3] W. Bao and C. Su, *A uniformly and optimally accurate method for the Zakharov system in the subsonic limit regime*, SIAM J. Sci. Comput. **40**, A929–A953 (2018).

[4] W. Bao, F. Sun and G.W. Wei, *Numerical methods for the generalized Zakharov system*, J. Comput. Phys. **190**, 201–228 (2003).

[5] J. Bourgain and J. Colliander, *On wellposedness of the Zakharov system*, Int. Math. Res. Not. **1996**, 515–546 (1996).

[6] Y. Cai et al., *A fourth-order compact finite difference scheme for the quantum Zakharov system that perfectly inherits both mass and energy conservation*, Appl. Numer. Math. **178**, 1–24 (2022).

[7] Y. Cai and Y. Yuan, *Uniform error estimates of the conservative finite difference method for the Zakharov system in the subsonic limit regime*, Math. Comp. **87**, 1191–1225 (2018).

[8] Q.S. Chang, B.L. Guo and H. Jiang, *Finite difference method for generalized Zakharov equations*, Math. Comp. **64**, 537–553 (1995).

[9] Q.S. Chang and H. Jiang, *A conservative difference scheme for the Zakharov equations*, J. Comput. Phys. **113**, 309–319 (1994).

[10] J. Colliander, *Wellposedness for Zakharov systems with generalized nonlinearity*, J. Differ. Equ. **148**, 351–363 (1998).
[11] R.T. Glassey, *Approximate solutions to the Zakharov equations via finite differences*, J. Comput. Phys. **100**, 377–383 (1992).
[12] R.T. Glassey, *Convergence of an energy-preserving scheme for the Zakharov equations in one space dimension*, Math. Comp. **58**, 83–102 (1992).
[13] H. Hadouaj, B.A. Malomed and G.A. Maugin, *Soliton-soliton collisions in a generalized Zakharov system*. Phys. Rev. A. **44**, 3932 (1991).
[14] H. Hadouaj, B.A. Malomed and G.A. Maugin, *Dynamics of a soliton in a generalized Zakharov system with dissipation*, Phys. Rev. A. **44**, 3925 (1991).
[15] S. Jin, P.A. Markowich and C. Zheng, *Numerical simulation of a generalized Zakharov system*, J. Comput. Phys. **201**, 376–395 (2004).
[16] C. Kenig, G. Ponce and L. Vega, *On the Zakharov and Zakharov-Schulman systems*, J. Funct. Anal. **127**, 204–234 (1995).
[17] R. Kress, *Numerical analysis*, Springer-Verlag (1998).
[18] X.G. Li, Y. Cai and P. Wang, *Operator-compensation methods with mass and energy conservation for solving the Gross-Pitaevskii equation*, Appl. Numer. Math. **151**, 337–353 (2020).
[19] N. Masmoudi and K. Nakanishi, *Energy convergence for singular limits of Zakharov type systems*, Invent. Math. **172**, 535–583 (2008).
[20] F. Merle, *Blow-up results of virial type for Zakharov equations*, Commun. Math. Phys. **175**, 433–455 (1996).
[21] P.K. Newton, *Wave interactions in the singular Zakharov system*, J. Math. Phys. **32**, 431–440 (1991).
[22] G.L. Payne, D.R. Nicholson and R.M. Downie, *Numerical solution of the Zakharov equations*, J. Comput. Phys. **50**, 482–498 (1983).
[23] C. Su, *Comparison of numerical methods for the Zakharov system in the subsonic limit regime*, J. Comput. Appl. Math. **330**, 441–455 (2018).
[24] C. Sulem and P.L. Sulem, *Regularity properties for the equations of Langmuir turbulence*, CR Acad. Sci. Paris Sér. A Math. **289**, 173–176 (1979).
[25] J. Wang, *Multisymplectic numerical method for the Zakharov system*, Comput. Phys. Commun. **180**, 1063–1071 (2009).
[26] Y. Xia, Y. Xu and C.W. Shu, *Local discontinuous Galerkin methods for the generalized Zakharov system*, J. Comput. Phys. **229**, 1238–1259 (2010).
[27] V.E. Zakharov, *Collapse of Langmuir waves*, Sov. Phys. JETP. **35**, 908–914 (1972).